Springer

KSME

Journal of Mechanical Science and Technology 28 (5) (2014) 1819~1831
www.springerlink.com/content/1738-494x
DOI 10.1007/s12206-014-0329-6

Numerical analysis of entropy generation in nanofluid flow over a transparent plate in porous medium in presence of solar radiation, viscous dissipation and variable magnetic field †

Mohammad Dehsara[1], Nemat Dalir[2,*] and Mohammad Reza Heirani Nobari[1]

[1]*Department of Mechanical Engineering, Amirkabir University of Technology , 424 Hafez Avenue, P.O. Box 15875-4413, Tehran, Iran*
[2]*Department of Mechanical Engineering, Salmas Branch, Islamic Azad University, Salmas, Iran*

(Manuscript Received September 11, 2012; Revised October 29, 2013; Accepted December 30, 2013)

Abstract

The entropy generation of magneto-hydrodynamic mixed convection flow of nanofluid over a nonlinear stretching inclined transparent plate embedded in a porous medium due to solar radiation is investigated numerically. The nanofluid is made of Cu nanoparticles with water as the base fluid. The two-dimensional governing equations, in presence of the effects of viscous dissipation, variable magnetic field and solar radiation are transformed by similarity method to two coupled nonlinear ODEs and then solved using the numerical implicit Keller-Box method. The effects of various parameters such as nanoparticle volume fraction, magnetic parameter, porosity, effective extinction coefficient of porous medium, diameter of porous medium solid particles and Eckert, Brinkman and Hartman numbers is investigated on velocity, temperature and entropy generation number profiles. The results reveal that near to the plate surface the increase of nanoparticle volume fraction, porosity and porous medium geometric parameter cause the entropy generation number to increase, but far enough from the plate surface the increase of nanoparticle volume fraction, porosity and porous medium geometric parameter cause the entropy generation number to decrease. Also the entropy generation number increases with the increase of Brinkman number and Hartman number, and this increase is dominant near the plate surface. Closer to the plate surface the reduction of Eckert number causes the increase of entropy generation number, but the entropy generation number increases with the increase of Reynolds number.

Keywords: Entropy generation; Inclined plate; Mixed convection; Nanofluid; Porous medium

1. Introduction

Fluid convection through porous medium has become one of the interesting subjects in heat transfer field in the last three decades. Studies show that the presence of porous medium enhances the thermal conditions. Moreover, another subject in heat transfer field which has been considerably taken into account by scientists and engineers is the use of nanofluids for thermal conductivity enhancement and finally increasing the convective heat transfer rate. The convective heat transfer of fluid over an inclined plate which is embedded in a porous medium due to solar radiation has various applications such as petroleum material production, separation processes in chemical engineering, thermal insulation systems and buildings.

Bejan and Polikakos [1] investigated the natural convection boundary layer in porous medium for non-Darcian regime. The mixed convection boundary layer flow over a vertical plate in a porous medium was analyzed by Merkin [2]. Chamkha [3] investigated the natural convection flow in porous medium with uniform porosity due to solar radiation. The MHD mixed convection flow over a vertical porous plate in a saturated porous medium and assuming non-Darcian model was studied by Takhar and Beg [4]. Sunder et al. [5] studied MHD natural convection-radiation interaction along a vertical surface embedded in a Darcian porous medium in presence of Soret and Dufour's effects. Ranganathan and Viskanta [6] investigated the fluid mixed convective boundary layer over a vertical plate embedded in porous medium. They claimed that the viscous effects are significant and cannot be neglected. Forced convection boundary layer flow over a vertical plate in a porous medium was studied by Murthy et al. [7] with a non-Darcian model.

The nanofluid heat transfer area has been given much attention by scientists in recent years. The fluids such as water, oil and ethylene glycol mixture have low convective heat transfer coefficient which is due to their low thermal conductivity. Therefore, recent studies have tried to enhance the convective heat transfer coefficient by adding nano or micro particles to the fluid. Choi [8] was the first who worked on this subject.

*Corresponding author. Tel.: +98 9376121607, Fax.: +98 2166952281
E-mail address: dalir@aut.ac.ir
† Recommended by Associate Editor Seungho Park

Choi et al. [9] showed that the addition of a few nanoparticles to the flowing fluid causes the thermal conductivity enhancement. Recently several works have investigated the nanofluid natural convection such as Ghasemi et al. [10] who studied the Cu-water nanofluid natural convection over an inclined surface. S. E. B. Maiga et al. [11] investigated the nanofluid effect on forced convection heat transfer. In a paper by X.Q. Wang [12], the performed numerical analyses on nanofluid flow and heat transfer have been reported. Habibi Matin et al. [13] investigated numerically the mixed convection taking into account the effects of MHD flow of nanofluid over a nonlinear stretching sheet and viscous dissipation. Noghrehabadi et al. [14] analyzed the boundary layer heat transfer and entropy generation of a nanofluid over an isothermal linear stretching sheet with heat generation/absorption and partial slip. In the last decade, the nanofluid convection heat transfer problem in porous medium has been given more attention by researchers. For example, Ahmad and Pop [15] studied the mixed convective boundary layer flow over a vertical plate embedded in a porous medium filled with a nanofluid. In the recent years, the entropy generation analysis of various flows has also been performed for some cases. Dehsara and coworkers [16] investigated numerically the entropy generation in the magneto-hydrodynamic (MHD) mixed convection flow over a nonlinear stretching inclined transparent plate embedded in a porous medium due to solar radiation. S. Aboud and S. Saouli [17] applied the entropy generation analysis to viscoelastic magneto-hydrodynamic (MHD) flow over a stretching surface. M. H. Yazdi et al. [18] presented a new design of open parallel micro-channels embedded within a permeable continuous moving surface in magneto-hydrodynamic (MHD) flow at a prescribed surface temperature using the entropy generation analysis. Nobari et al. [19] studied numerically the entropy analysis in mixed convection MHD flow of nanofluid over a non-linear stretching sheet taking into account the effects of viscous dissipation and variable magnetic field. Therefore, it should be said that in spite of the attention to the nanofluid convection flow and heat transfer problems through porous media by researchers in the last decade, the entropy generation analysis of nanofluid flow in porous media has not been given much attention by researchers, such that only a few studies have investigated this subject. Thus the present paper aims to fill the available gap between studies of mixed convection flow of nanofluid in porous media and entropy generation analyses.

The present paper studies the entropy generation analysis of magneto hydrodynamic (MHD) mixed convection flow of nanofluid over a non-linearly stretching inclined transparent plate embedded in a porous medium with uniform porosity due to solar radiation. The boundary layer equations have been transformed by similarity transformation to two coupled non-linear ordinary differential equations. These equations are reduced to five first order nonlinear ordinary differential equations and then are solved using an implicit numerical method called Keller-Box. The effects of various parameters are studied on the dimensionless velocity, temperature and entropy generation number profiles.

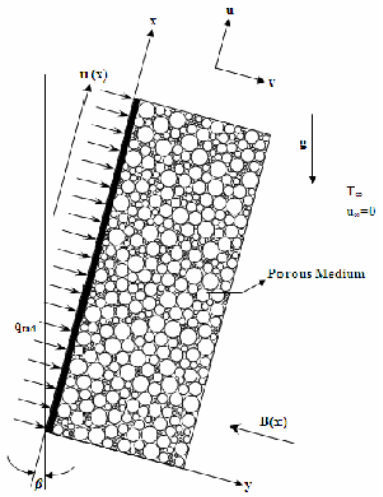

Fig. 1. Schematic of the physical model and system coordinates.

2. Mathematical formulation

Steady-state two-dimensional boundary layer mixed convection MHD flow of nanofluid is considered over a smooth non-linearly stretching inclined transparent plate embedded in a porous medium with uniform porosity in presence of solar radiation, viscous dissipation and variable magnetic field. An incompressible nanofluid with electrical conductivity in presence of magnetic field $B(x)$, perpendicular to the plate, is considered. Fig. 1 shows the schematics of the physical model and system coordinates.

It is assumed that x and y coordinates are the flow directions along the plate and perpendicular to the plate, respectively. The plate temperature (T_w) is assumed constant and is considered higher than ambient temperature (T_∞). The base fluid of the nanofluid, i.e., water, has Prandtl number of $Pr = 6.2$. The nanoparticles added to the base fluid (water) are copper (Cu) particles. The porous medium is assumed to be transparent and in thermal equilibrium with the fluid. The base fluid and the nanoparticles are assumed to be in thermal equilibrium and no slip occurs between them. Assuming incompressible viscous nanofluid and steady-state laminar two-dimensional flow and Boussinesq approximation in presence of solar radiation, viscous dissipation and magnetic field, the governing differential equations are as follows [20, 21]:

$$\frac{\partial u}{\partial x}+\frac{\partial v}{\partial y}=0 \tag{1}$$

$$u\frac{\partial u}{\partial x}+v\frac{\partial u}{\partial y}=\frac{\mu_{\mathrm{nf}}}{\rho_{\mathrm{nf}}}\frac{\partial^2 u}{\partial y^2}-\frac{\mu_{\mathrm{nf}}}{\rho_{\mathrm{nf}}K(\varepsilon)}u-C(\varepsilon)u^2 -\frac{\sigma B(x)^2}{\rho_{\mathrm{nf}}}u+\frac{g(\rho\beta^t)_{\mathrm{nf}}}{\rho_{\mathrm{nf}}}(T-T_\infty)\cos(\beta) \tag{2}$$

$$u\frac{\partial T}{\partial x}+v\frac{\partial T}{\partial y}=\frac{k_{\mathrm{ef}}}{(\rho C_{\mathrm{p}})_{\mathrm{nf}}}\frac{\partial^2 T}{\partial y^2}+\frac{1}{(\rho C_{\mathrm{p}})_{\mathrm{nf}}}\frac{\partial q_{\mathrm{rad}}}{\partial \mathrm{y}}+\frac{\mu_{\mathrm{nf}}}{(\rho C_{\mathrm{p}})_{\mathrm{nf}}}\left(\frac{\partial u}{\partial y}\right)^2 . \tag{3}$$

The boundary conditions are as follows:

$$\begin{aligned} &u=u_{\mathrm{w}}(x)=bx^{\mathrm{m}}, v=0, T=T_{\mathrm{w}},\ at\ y=0\\ &u\to 0, T\to T_{\infty},\ at\ y\to\infty \end{aligned} \tag{4}$$

where b is a constant, u and v are fluid velocity components in x and y directions respectively, σ is the electrical conductivity, β is the plate inclination angle, and μ_{nf}, ρ_{nf} and $\beta^{t}{}_{\mathrm{nf}}$ are the effe ctive dynamic viscosity, effective density and effective thermal expansion coefficient of the nanofluid respectively, which are considered in the following relations [22]:

$$\rho_{\mathrm{nf}}=\varphi\rho_{\mathrm{s}}+(1-\varphi)\rho_{\mathrm{f}} \tag{5}$$

$$\mu_{\mathrm{nf}}=\frac{\mu_{\mathrm{f}}}{(1-\varphi)^{2.5}} \tag{6}$$

$$(\rho\beta^{t})_{\mathrm{nf}}=(1-\varphi)(\rho\beta^{t})_{\mathrm{f}}+\varphi(\rho\beta^{t})_{\mathrm{s}} . \tag{7}$$

Here φ is the solid nanoparticles volume fraction, μ_{f} is the basic fluid dynamic viscosity, and $\beta^{t}{}_{\mathrm{f}}$ and $\beta^{t}{}_{\mathrm{s}}$ are thermal expansion coefficients of the basic fluid and nanoparticles respectively. ε is the porosity and ρ_{f}, ρ_{s}, $(C_p)_{\mathrm{f}}$ and $(C_p)_{\mathrm{s}}$ are the basic fluid density, nanoparticles density, the basic fluid specific heat and the nanoparticles specific heat. Also $K(\varepsilon)$ and $C(\varepsilon)$ are the porous medium permeability and inertia coefficient which are defined by the following relations for uniform porosity [23]:

$$K(\varepsilon)=\frac{d_{\mathrm{p}}^2\varepsilon^3}{175(1-\varepsilon)^2} \tag{8}$$

$$C(\varepsilon)=\frac{1.75(1-\varepsilon)}{d_{\mathrm{p}}\varepsilon^2} . \tag{9}$$

ε is the porosity of porous medium which is constant assuming uniform distribution of solid components and d_{p} is the diameter of porous medium solid particles. k_{ef} is the effective thermal conductivity of porous medium, from which Pr is obtained and q_{rad} is the solar radiation flux. Assuming that some of the solar radiation reaching the plate surface is absorbed by the fluid, the Beer law can be used for radiation absorption and written as:

$$q''(y)=q''(0)(1-e^{-ay}) \tag{10}$$

where $q''(y)$ is the radiation flux reached to distance y from the transparent plate, $q''(0)$ is the incident flux to the plate and a is the extinction coefficient of the nanofluid. Also here the variable magnetic field is considered as follows [24]:

$$B(x)=B_0x^{\left(\frac{\mathrm{m}-1}{2}\right)} \tag{11}$$

where $B(x)$ is the strength of the variable magnetic field. The special form of the magnetic field, i.e. Eq. (11), is chosen to obtain a similarity solution. This form of $B(x)$ has also been considered in Refs. [24, 25] in their MHD flows past a moving or fixed flat plate. Similarity variable used to transform governing equations to ordinary differential equations is:

$$\eta=\frac{y}{x}\left(\frac{m+1}{2}\right)^{\frac{1}{2}}(\mathrm{Re}_{\mathrm{x}})^{\frac{1}{2}} \tag{12}$$

where:

$$\mathrm{Re}_{\mathrm{x}}=\frac{\rho_f u_{\mathrm{w}}(x)}{\mu_f}x . \tag{13}$$

Dimensionless stream function and temperature are as follows:

$$f(\eta)=\frac{\psi(x,y)(\mathrm{Re}_{\mathrm{x}})^{\frac{1}{2}}}{u_{\mathrm{w}}(x)} \tag{14}$$

$$\theta(\eta)=\frac{T-T_{\infty}}{T_{\mathrm{w}}-T_{\infty}} \tag{15}$$

such that the stream function satisfies the continuity equation:

$$u=\frac{\partial\psi}{\partial y},\ v=-\frac{\partial\psi}{\partial x} . \tag{16}$$

By substitution of similarity parameters in momentum and energy equations, governing equations take following forms:

$$\begin{aligned} &f_{\eta\eta\eta}+(1-\varphi)^{2.5}\left((1-\varphi)+\varphi\left(\frac{\rho_{\mathrm{s}}}{\rho_{\mathrm{f}}}\right)\right)\left(\frac{m+1}{2}\right)^2.ff_{\eta\eta}\\ &-(1-\varphi)^{2.5}\left((1-\varphi)+\varphi\left(\frac{\rho_{\mathrm{s}}}{\rho_{\mathrm{f}}}\right)\right).\left(m+\frac{1.75(1-\varepsilon)}{d_{\mathrm{p}}\varepsilon^2}\right).f_{\eta}^2\\ &-\left(\frac{175(1-\varepsilon)^2}{d_{\mathrm{p}}^2\varepsilon^2.Re}+(1-\varphi)^{2.5}Mn\right).f_{\eta}\\ &+(1-\varphi)^{2.5}\left((1-\varphi)+\varphi\left(\frac{(\rho C_{\mathrm{p}})_{\mathrm{s}}}{(\rho C_{\mathrm{p}})_{\mathrm{f}}}\right)\right).\left(\frac{Gr}{Re^2}\right)\cos(\beta).\theta=0 \end{aligned} \tag{17}$$

$$\begin{aligned} &\theta_{\eta\eta}+\left((1-\varphi)+\varphi\left(\frac{(\rho C_{\mathrm{p}})_{\mathrm{s}}}{(\rho C_{\mathrm{p}})_{\mathrm{f}}}\right)\right)Pr.f\theta_{\eta}\\ &+\frac{Ec.Pr}{(1-\varphi)^{2.5}}.f_{\eta\eta}^2+\frac{R}{Re}.exp\left(\frac{-a_e\eta}{\sqrt{Re}}\right)=0 . \end{aligned} \tag{18}$$

And the boundary conditions become:

$$f_\eta = 1, f = 0, \theta = 1, \text{ at } \eta = 0$$
$$f_\eta \to 0, \theta \to 0, \text{ as } \eta \to \infty \tag{19}$$

where R, a_e, Mn, D_p, Re_x, Pr, Ec, Gr/Re_x^2 are the radiation parameter, extinction (absorption) parameter, magnetic parameter, porous medium geometric parameter and dimensionless Reynolds, Prandtl, Eckert and Richardson numbers respectively, which are defined as:

$$\frac{Gr}{\mathrm{Re_x}^2} = \frac{g(T_\mathrm{w} - T_\infty)\beta_f'}{u_\mathrm{w}(x)^2 x^2},\ \mathrm{Re}_x = \frac{u_\mathrm{w}(x)}{\upsilon_f}x,\ a_e = ax,$$
$$D_p = \frac{d_p}{x},\ Ec = \frac{u_\mathrm{w}(x)^2}{C_\mathrm{p}(T_\mathrm{w} - T_\infty)},\ \mathrm{Pr} = \frac{(\rho C_\mathrm{p})_\mathrm{f}}{k_\mathrm{ef}}\upsilon_f,$$
$$Mn = \frac{\sigma B_0^2}{\rho_f b},\ R = Nu_r a_e,\ Nu = -\sqrt{\frac{m+1}{2}\mathrm{Re_x}}\,\theta_\eta(0),$$
$$C_\mathrm{f} = -\sqrt{\frac{2(m+1)}{\mathrm{Re_x}}} f_{\eta\eta}(0)\,. \tag{20}$$

3. Entropy generation analysis

The local volumetric rate of entropy generation in the presence of a magnetic field is given by the following relation [26]:

$$S_G = \frac{k_\mathrm{ef}}{T_\infty^2}\left(\left(\frac{\partial T}{\partial x}\right)^2 + \left(\frac{\partial T}{\partial y}\right)^2\right)$$
$$+\frac{\mu_{nf}}{T_\infty}\left(\frac{\partial u}{\partial y}\right)^2 + \frac{\sigma.B(x)^2}{T_\infty}u^2 \tag{21}$$

where the first term on the right-hand side of Eq. (21) is the entropy generation due to heat transfer across a finite temperature difference; the second term is the entropy generation due to viscous dissipation, and the third term is the entropy generation due to the magnetic field effect. Here it is appropriate to define a dimensionless number for entropy generation rate, N_s. The ratio of the local volumetric entropy generation rate, S_G, to a characteristic entropy generation rate, $(S_G)_0$ is defined as the entropy generation number. The characteristic entropy generation rate can be written as:

$$(S_G)_0 = k_{ef}\left(\frac{\Delta T}{xT_\infty}\right)^2. \tag{22}$$

Thus the entropy generation number is written as:

$$N_s = \frac{S_G}{(S_G)_0}. \tag{23}$$

By the use of Eqs. (12)-(14) and (21), entropy generation number is given by the following relation in terms of the dimensionless velocity and temperature variables:

$$N_s = \frac{Br.Re}{\Omega}.f_{\eta\eta}^2 + \frac{Br.(Ha)^2}{\Omega}.f_\eta^2 + Re.\theta_\eta^2 \tag{24}$$

in which Re_x, Br, Ω and Ha are the Reynolds number, Brinkman number, the dimensionless temperature difference and the Hartman number respectively. These dimensionless numbers are given by the following relations:

$$Br = \frac{\mu_{nf}.u_w^2}{k_{ef}.\Delta T}, \Omega = \frac{\Delta T}{T_\infty}, Ha = B_0 x\left(\frac{\sigma}{\mu_{nf}}\right)^{\frac{1}{2}}. \tag{25}$$

4. Solution methodology

The nonlinear coupled ordinary differential equations derived by the similarity method, Eqs. (17) and (18), subject to the boundary conditions Eq. (19) are solved numerically using an implicit efficient finite difference scheme known as the Keller-Box method. The method has the following four main steps: (i) The system of Eqs. (17) and (18) are reduced to a first order system; (ii) The difference equations are written using central differences; (iii) The resulting algebraic equations are linearized by Newton's method and written in matrix vector form; (iv) The block-tridiagonal-elimination technique is used to solve the linear system. The details of the Keller-Box method can be found in Ref. [27]. In order to satisfy the 10^{-4} convergence criterion, a step size of $\Delta\eta = 0.005$ is chosen in all cases. It is seen in solution that $\eta_\infty = 10$ is adequate for applying the perfect influence of the boundary layer.

5. Results and discussion

In the present study, the steady state two-dimensional boundary layer magneto-hydrodynamic mixed convection flow of nanofluid is considered over a smooth non-linearly stretching inclined transparent plate embedded in a porous medium due to solar radiation and with viscous dissipation and variable magnetic field. The dimensionless velocity, temperature and entropy generation number profiles are plotted for various values of governing parameters and are discussed in details. Some tables are also presented for Nusselt number Nu and skin friction coefficient C_f.

Tables 1 and 2 present the values of Nu number and skin friction coefficient for various values of physical parameters. Fluid and nanoparticles properties are also given in Table 3.

Fig. 2 shows the dimensionless velocity profiles for various values of porosity and nanoparticles volume fraction. As it can be seen, the porosity increase causes the increase of velocity in the boundary layer because when the porosity boosts the fluid can move with more freedom and fewer barriers resisting the momentum transfer along the plate. In contrast, when the na-

Table 1. Skin friction coefficient and Nusselt number for various values of the physical parameters: $m = 1.0$, $Pr = 6.2$, $x = 0.10$, $Re = 500$, $D_p = 20$, $Nu_r = 10$.

Ec	a_e	φ	Mn	β	Gr/Re^2	ε = 0.1		ε = 0.2		ε = 0.3	
						C_f	Nu	C_f	Nu	C_f	Nu
0	0.5	0.2	0.1	0	0.1	0.2517	9.3400	0.1213	11.9048	0.0798	13.1458
					1.0	0.2400	10.0824	0.1027	12.7836	0.0571	14.0872
					10	0.1423	13.0653	0.0436	16.4664	0.1174	18.1121
0.1	1	0.1	0	30	0.1	0.2428	6.0508	0.1172	10.2613	0.0775	11.9652
					1	0.2283	7.3768	0.0944	11.7393	0.0497	13.4611
					10	0.1105	12.5287	0.0810	16.2607	0.1610	16.9225
1	0	0	0.2	90	0.1	0.2114	9.5346	0.1079	2.9784	0.0769	6.7887
					1	0.2113	9.5279	0.1078	2.9851	0.0769	6.7976
					10	0.2111	9.4541	0.1075	3.0590	0.0765	6.8692

Table 2. Skin friction coefficient and Nusselt number for various values of the physical parameters: $m = 1.0$, $Pr = 6.2$, $x = 0.10$, $Re = 500$, $Nu_r = 10$.

Ec	a_e	Mn	β	Gr/Re^2	D_p	ε = 0.1		ε = 0.2		ε = 0.3	
						C_f	Nu	C_f	Nu	C_f	Nu
0	0.5	0.1	0	0.1	10	0.2936	8.4568	0.1394	11.7260	0.0893	13.1704
					15	0.2388	9.7582	0.1143	12.4124	0.0747	13.6646
					20	0.2066	10.3060	0.0997	12.8484	0.0664	13.9575
0.1	1	0	30°	1	10	0.2758	7.1151	0.1100	11.7438	0.0518	13.8055
					15	0.2182	8.5552	0.0814	12.7366	0.0338	14.4785
					20	0.1838	9.4965	0.0643	13.3515	0.0232	14.8743
0.2	0	0	90°	10	10	0.2944	3.2065	0.1399	9.6732	0.0892	12.1485
					15	0.2395	5.6751	0.1146	10.8807	0.0741	12.9423
					20	0.2073	6.8893	0.0998	11.6163	0.0655	13.4030

Table 3. Thermo-physical properties of water and nanoparticles [28].

Physical properties	Fluid phase (water)	Cu
ρ (kg.m^{-3})	997.1	8933
C_p(J.kg^{-1}.K^{-1})	4179	385
$\beta^t \times 10^5$ (K^{-1})	21.0	1.67
k (W.m^{-1}.K^{-1})	0.613	401

noparticles volume fraction increases, the velocity in the boundary layer decreases, and this is due to more collisions between solid particles which causes the reduction of nanofluid effective velocity. Thus, according to Fig. 2, it can be claimed that the porosity of porous medium and nanoparticles volume fraction have considerable effect on the hydrodynamic boundary layer.

Fig. 3 shows the effect of radiation Nusselt number parameter on dimensionless velocity profile for various values of porosity. It can be seen that the radiation flux magnitude does not have considerable effect on velocity profile.

Fig. 4 shows the effect of Eckert number on velocity profile for some values of nanoparticles volume fraction. It can be seen that the increase of Eckert number causes the increase of velocity magnitude inside the porous medium. Moreover, with

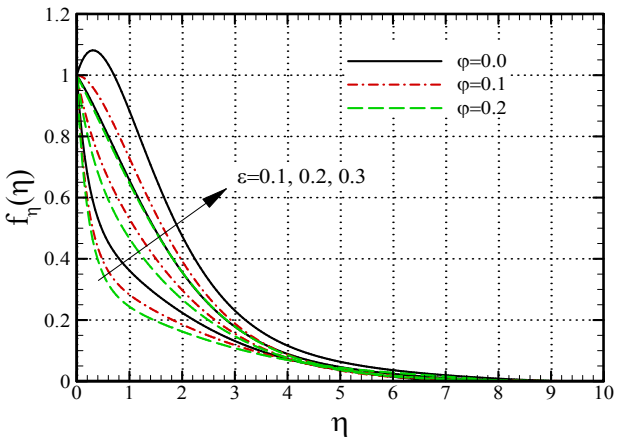

Fig. 2. Dimensionless velocity profiles for different values of porosity and volume fraction: $Mn = 0.1$, $Ec = 0.2$, $Gr/Re^2 = 4$, $\beta = 0$.

the decrease of nanoparticles volume fraction the maximum velocity point shifts from the plate surface to further distances of the plate.

The effect of Richardson number Gr/Re_x^2 on the velocity profile has been shown in Fig. 5 for various values of porosity. As it is expected when the Richardson number increases, the

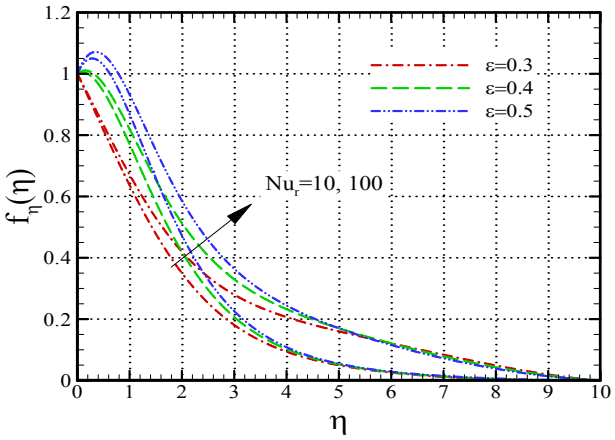

Fig. 3. Dimensionless velocity profiles for different values of porosity and Nusselt number: $Mn = 0.1$, $\varphi = 0.2$, $Gr/Re^2 = 4$, $\beta = 0$.

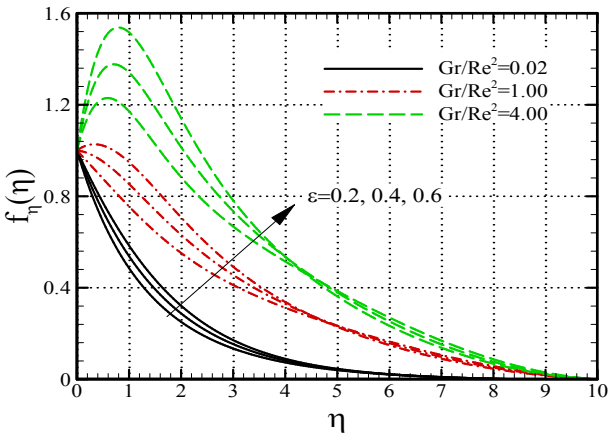

Fig. 5. Dimensionless velocity profiles for different values of porosity and Richardson number: $Nu_r = 100$, $a_e = 0.2$, $\varphi = 0.1$, $\beta = 0$.

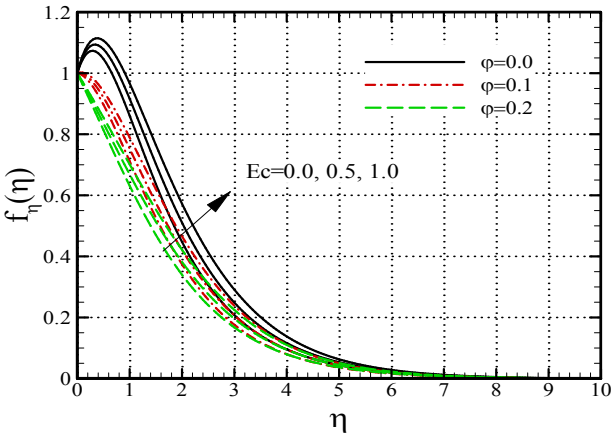

Fig. 4. Dimensionless velocity profiles for different values of volume fraction and Eckert number: $Mn = 0.1$, $\varepsilon = 0.3$, $Gr/Re^2 = 4$, $\beta = 0$.

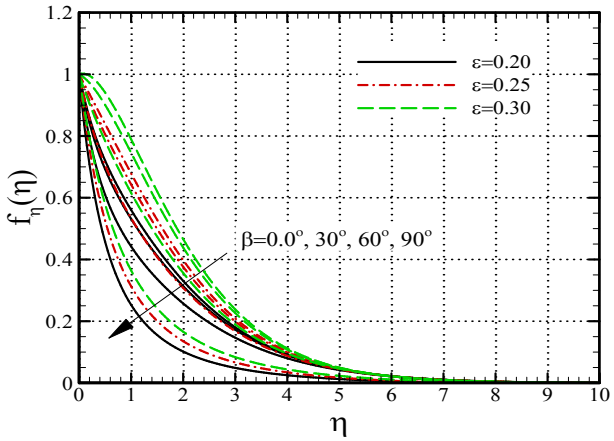

Fig. 6. Dimensionless velocity profiles for different values of porosity and plate inclination angle: $\varphi = 0.1$, $Ec = 1$, $Gr/Re^2 = 4$, $Mn = 0.1$.

hydrodynamic boundary layer thickness increases because when the Richardson number increases, the natural convection dominates the forced convection and the buoyancy forces play more effective role than the friction forces. The interesting point which should be mentioned is that in higher values of Richardson number the porosity has greater effect on velocity profile, i.e. using the porous medium is more effective in natural convection conditions than the forced convection conditions. Also it can be seen that in higher porosity the friction effect continues to further distances of the plate while in small porosity the friction effect does not go far beyond the near points of the plate.

Fig. 6 shows the effect of transparent plate inclination angle on dimensionless velocity profile. It is seen that the decrease of the plate inclination angle with respect to verticality shifts the velocity profiles upper and this is because the more the plate goes to verticality, the easier the fluid can move over the plate and this is due to the increase in $\cos(\beta)$ term in the momentum equation which causes the fluid momentum to increase. Another point is that in the angle range of 0-30 degrees with respect to the horizontal state, there is the main increase in velocity profile and in the angles near to horizontal state, the variation of the inclination angle has negligible effect on velocity.

Fig. 7 shows the dimensionless velocity profiles for various values of nanoparticle volume fraction and effective extinction coefficient. It can be seen that at a constant nanoparticle volume fraction the dimensionless velocity profiles shift upper with the increase of the effective extinction coefficient, i.e., the dimensionless velocity boundary layer becomes thicker with the increase of the effective extinction coefficient. Also it is seen that the increase of nanoparticle volume fraction causes the increase of velocity boundary layer thickness for a constant effective extinction coefficient.

Fig. 8 shows the effect of nanoparticles volume fraction along with porosity on dimensionless temperature profile. As it is expected the reduction of porosity causes the increase of thermal boundary layer thickness and this is because the increase of the ratio of solid particles in porous medium (decrease of porosity) resists the movement of nanofluid and this

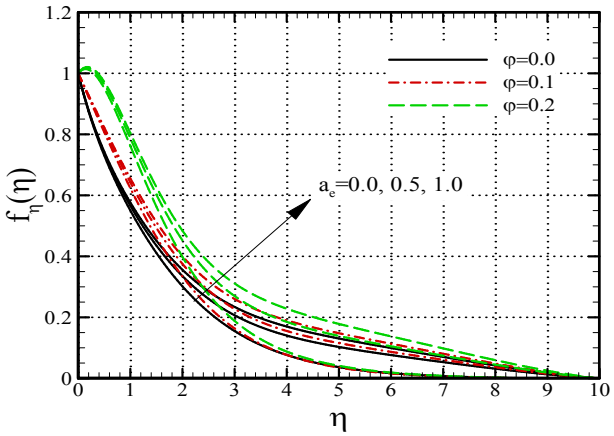

Fig. 7. Dimensionless velocity profiles for different values of nanoparticle volume fraction and effective extinction coefficient: $D_p = 10$, $Nu_r = 100$, $\beta = 0$, $Gr/Re^2 = 4$.

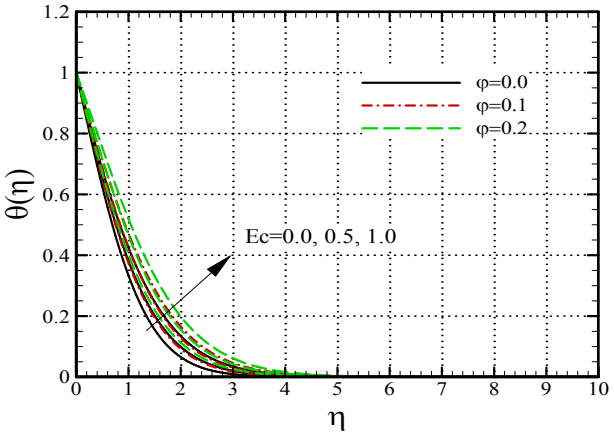

Fig. 9. Dimensionless temperature profiles for different values of volume fraction and Eckert number: $Mn = 0.1$, $\varepsilon = 0.3$, $Gr/Re^2 = 4$, $\beta = 0$.

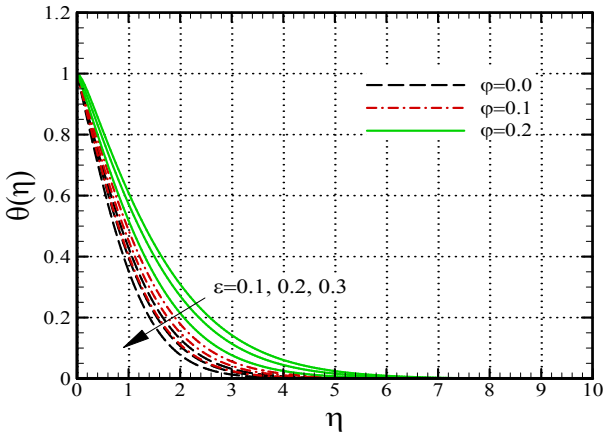

Fig. 8. Dimensionless temperature profiles for different values of porosity and volume fraction: $Mn = 0.1$, $Ec = 0.2$, $Gr/Re^2 = 4$, $\beta = 0$.

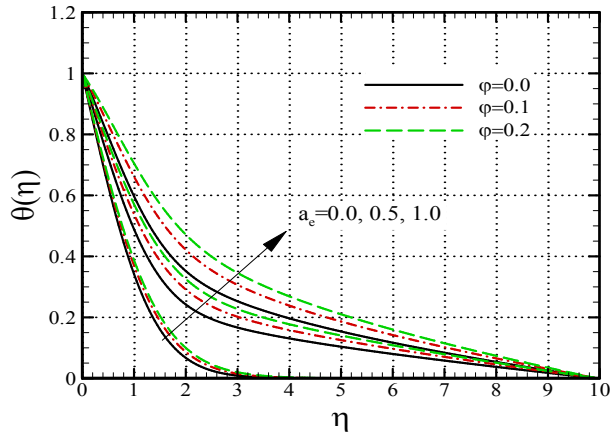

Fig. 10. Dimensionless temperature profiles for different values of volume fraction and effective extinction coefficient: $D_p = 10$, $Nu_r = 100$, $\beta = 0$, $Gr/Re^2 = 4$.

result in warmer nanofluid and thicker thermal boundary layer. By the way, the increase of nanofluid volume fraction has an enhancement effect on temperature and this is in fact the reason for using nanofluid because the existence of nanoparticles increases the effective thermal conductivity and finally thickens the boundary layer.

The dimensionless temperature profile is plotted for various values of Eckert number and nanoparticles volume fraction in Fig. 9. It is obvious that the increase of Eckert number causes the increase of nanofluid temperature in thermal boundary layer and physically this can be totally verified, because when the friction on the plate increases due to fluid viscosity, more heat is generated and as a result the nanofluid temperature increases.

The influence of effective absorption coefficient of porous medium containing nanofluid on temperature profile is shown in Fig. 10. It can be observed that when the effective absorption coefficient increases, the boundary layer thickness increases and this is because when the effective absorption coefficient increases, the solar radiation flux by surroundings increases and as a result the nanofluid temperature increases. It should be noted that the presence of nanofluid and also the dark_color of solid particles of porous medium can enhance the effective absorption coefficient and finally the temperature of the thermal boundary layer.

Fig. 11 shows the effect of Richardson number on temperature for some values of porosity. It is seen that the temperature reduces in high Richardson numbers for which the natural convection flow is dominant. Fig. 12 shows the effect of radiation Nusselt number on temperature profile. It can be seen that when the dimensionless radiation Nusselt number increases, the temperature in the boundary layer increases.

The temperature profile is shown for various values of plate inclination angle in Fig. 13. It can be observed that when the plate goes to verticality, the temperature profiles shift upper. This is expected because in higher plate inclination angles the gravity acceleration component along the plate increases and ultimately the buoyancy effects appear.

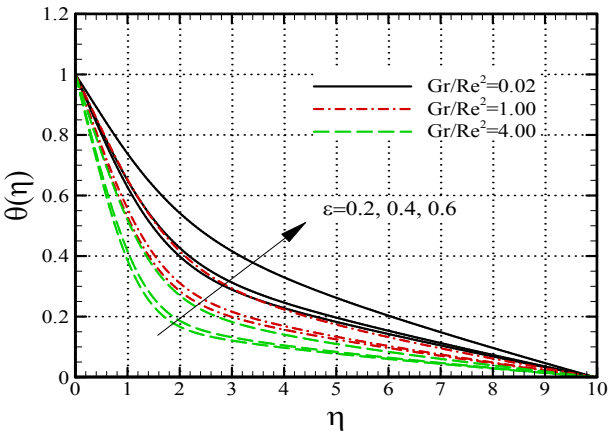

Fig. 11. Dimensionless temperature profiles for different values of porosity and Richardson number: $a_e = 0.5$, $Nu_r = 100$, $\varphi = 0.1$, $\beta = 0$.

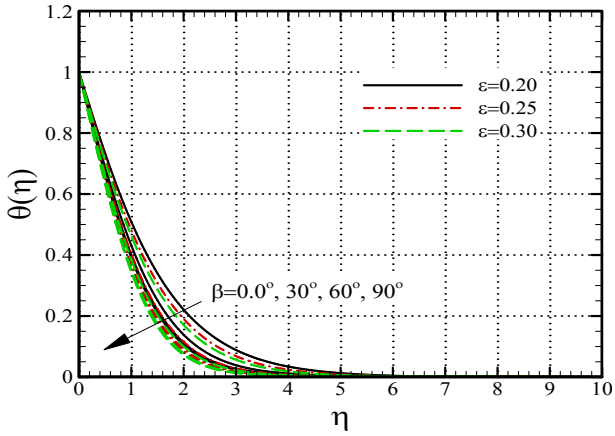

Fig. 13. Dimensionless temperature profiles for different values of porosity and plate inclination angle: $Mn = 0.1$, $\varphi = 0.1$, $a_e = 0.5$, $Gr/Re^2 = 4$.

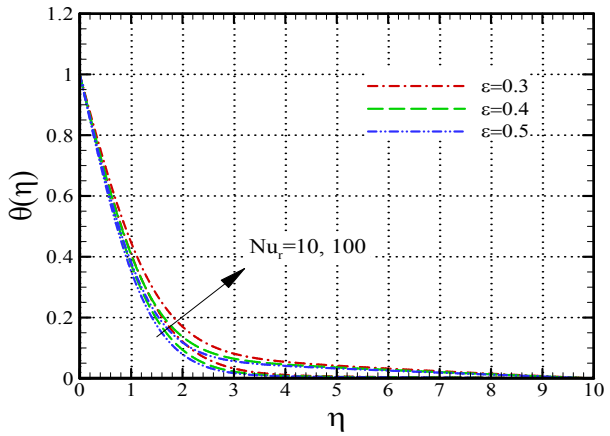

Fig. 12. Dimensionless temperature profiles for different values of porosity and plate Nusselt number: $Mn = 0.1$, $\varphi = 0.2$, $Gr/Re^2 = 4$, $a_e = 0.1$.

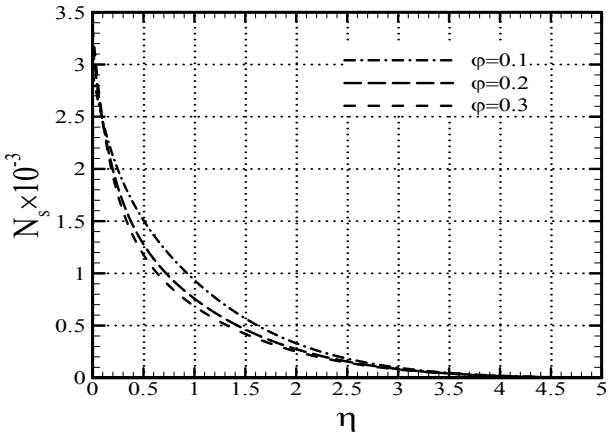

Fig. 14. Dimensionless entropy generation number profiles for different values of nanoparticle volume fraction: $Mn = 0.1$, $a_e = 0.5$, $Ec = 1.0$, $Re = 500$, $\varepsilon = 0.20$, $Ha = 50.0$, $Br\Omega^{-1} = 1.0$, $Pr = 6.2$.

The effects of various physical parameters on dimensionless entropy generation number profiles are shown in Figs. 14-22. Here it should be said that the dimensionless entropy generation number profiles of Figs. 14-22 are for the case of natural convection (with $Gr/Re^2 = 4.0$) of MHD flow of nanofluid over a nonlinearly stretching transparent plate embedded in a porous medium.

The dimensionless entropy generation number profiles for various values of nanoparticle volume fraction are shown in Fig. 14. It can be seen that the increase of nanoparticle volume fraction causes the dimensionless entropy generation number profiles to shift slightly downward for distances far from the plate surface. However, as the nanoparticle volume fraction increases, the entropy generation increases near the plate surface due to the higher dissipation energy resulted from the sharper velocity gradients near the plate surface. It can be seen that at distances close to the plate surface ($\eta \leq 0.15$) nanoparticle volume fraction increase causes entropy generation increase, but for distances far enough from plate surface ($\eta > 0.15$) nanoparticle volume fraction increase causes the entropy generation reduction.

Due to Fig. 14, at $\eta = 0$ when the nanoparticle volume fraction φ increases from 0.1 to 0.2, the entropy generation number N_s increases from 2924.0 to 3175.4, i.e., with 100% increase in φ, N_s increases 8.6%. At $\eta = 1$ the N_s reduces from 934.8 to 757.9 with the increase of φ from 0.1 to 0.2, which means 23.34% reduction in N_s by 100% increase in φ.

Fig. 15 shows the effect of porosity ε on dimensionless entropy generation number profile. It can be seen that the entropy generation on the plate surface and distances close to the plate ($\eta \leq 0.15$) increases with the increase of porosity. This is because when porosity increases, the possibility of free motion of the fluid particles inside porous medium increases. On the other hand, the fluid temperature increases (see Fig. 11) and this is another reason for the increase of fluid particles motions and consequently the irreversibility of the fluid. For $\eta > 0.15$ the increase of porosity causes the decrease of N_s.

It is seen from Fig. 15 that at $\eta = 0$ (on the plate surface)

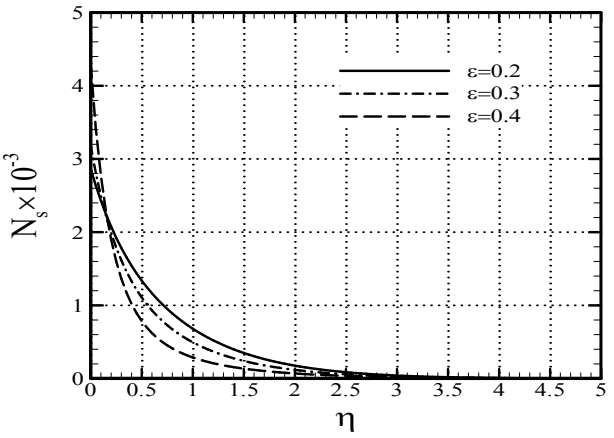

Fig. 15. Dimensionless entropy generation number profiles for different values of porosity: Mn = 0.1, φ = 0.1, a_e = 0.5, Re = 500, Ec = 1.0, Ha = 50.0, $Br\Omega^{-1}$ = 1.0, Pr = 6.2.

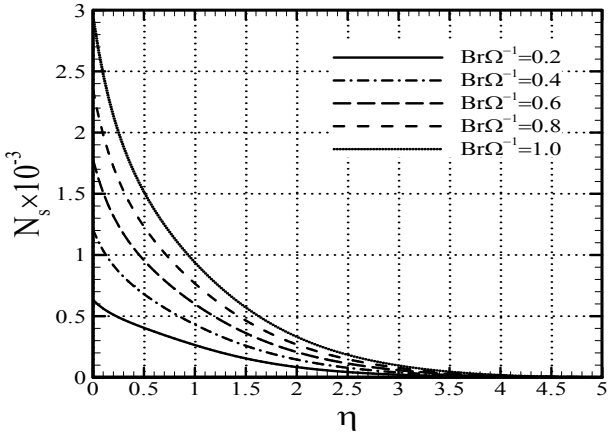

Fig. 16. Dimensionless entropy generation number profiles for different values of dimensionless group parameter: Mn = 0.1, φ = 0.1, a_e = 0.5, Re = 500, ε = 0.20, Ha = 50.0, Ec = 1.0, Pr = 6.2.

when the porosity ε increases from 0.2 to 0.4, the entropy generation number N_s increases from 2867.2 to 4286.0, which means 100% increase in porosity ε causes 49.48% increase of N_s. Also at η = 1 with the porosity increases from 0.2 to 0.4, the N_s decreases from 680.7 to 288.0, which means 100% increase in porosity ε causes 136.35% reduction in N_s.

Fig. 16 demonstrates the dimensionless entropy generation number profiles for different values of dimensionless group parameter $Br\Omega^{-1}$. It can be seen that, unlike the effective extinction coefficient, the variation of dimensionless group parameter shows a considerable effect on the dimensionless entropy generation number profiles. The dimensionless entro py generation number profiles shift upward (the N_s values increase) with the increase of the dimensionless group parameter, and this shifting upward is dominant in distances near to the plate surface. It can be said that by the increase of dimensionless group parameter, the fluid velocity increases which causes the fluid particles randomness level to increase.

It can also be seen in Fig. 16 that the entropy generation number is maximized on the plate surface. In these cases the surface acts as the strong source of irreversibility and randomness generation.

Due to Fig. 16, when the dimensionless group parameter $Br\Omega^{-1}$ increases from 0.4 to 0.8, the entropy generation number N_s increases from 431.7 to 767.1, which means the increase of 77.70% in N_s by 100% increase in $Br\Omega^{-1}$.

Fig. 17 indicates the effect of porous medium geometric parameter D_p on dimensionless entropy generation number profile. It is seen that for $\eta \leq 0.15$ the entropy generation number profiles move upward (N_s values increase) with the increase of the porous medium geometric parameter, but for $\eta > 0.15$ the entropy generation numbers decrease with the increase of porous medium geometric parameter. It can be seen that the variation of N_s values with D_p in Fig. 17 is consistent with the variation of N_s values with ε in Fig. 15 for both $\eta \leq 0.15$ and $\eta > 0.15$. The reason is that the increase of D_p (which is proportional to the diameter of porous medium particles) causes the increase of pores volume in the porous medium and therefore the increase of porosity.

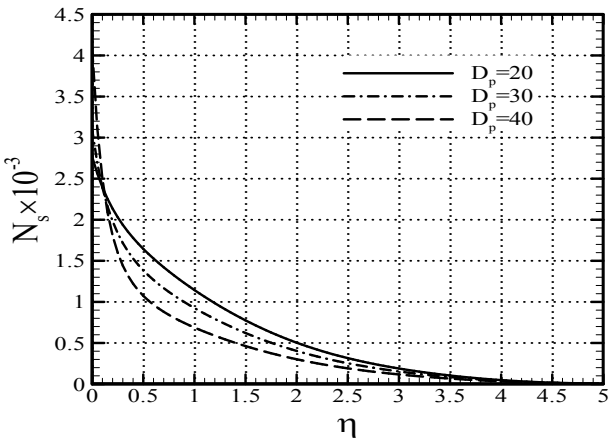

Fig. 17. Dimensionless entropy generation number profiles for different values of porous medium geometric parameter: Mn = 0.1, φ = 0.1, a_e = 0.5, Re = 500, ε = 0.20, Ha = 50.0, Ec = 1.0, Pr = 6.2.

According to Fig. 17, at η = 0 the N_s values boost from 4081.2 to 2766.2 by the increase of D_p from 20 to 40, which is 47.54% boost in N_s by 100% increase in D_p. At η = 1 the N_s values reduce from 1144.4 to 688.1 by the increase of D_p from 20 to 40, which is 66.31% reduction in N_s by 100% increase of D_p.

The N_s profiles for various values of Hartman number (Ha) are demonstrated in Fig. 18. It can be seen that the higher values of Hartman number produce higher entropy generation numbers at a specific distance from the plate surface and this is observable by upward shifted N_s profiles with the increase of Hartman number. The increase of Hartman number means the increase of magnetic field on the plate and porous medium, for which this increase of the resultant force from magnetic field causes the increase of fluid temperature particularly and

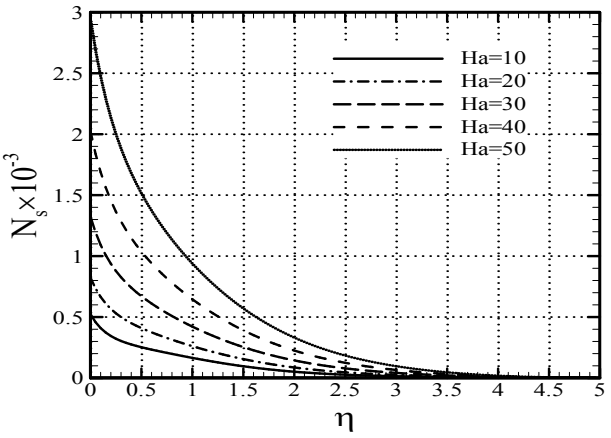

Fig. 18. Dimensionless entropy generation number profiles for different values of Hartman number: $Mn = 0.1$, $\varphi = 0.1$, $a_e = 0.5$, $Re = 500$, $\varepsilon = 0.20$, $Ec = 1.0$, $Br\Omega^{-1} = 1.0$, $Pr = 6.2$.

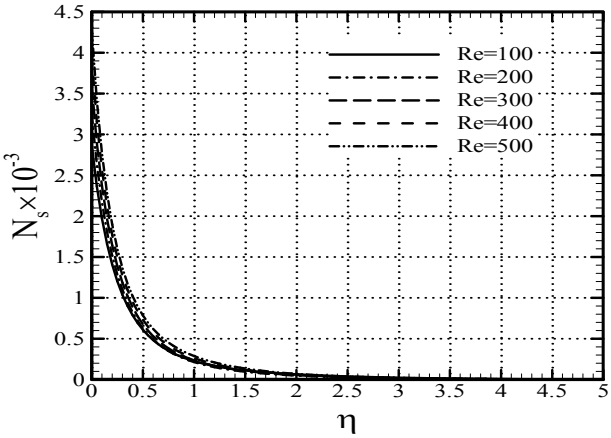

Fig. 19. Dimensionless entropy generation number profiles for different values of Reynolds number: $Mn = 0.1$, $\varphi = 0.1$, $a_e = 0.5$, $Ec = 1.0$, $\varepsilon = 0.20$, $Ha = 50.0$, $Br\Omega^{-1} = 1.0$, $Pr = 6.2$.

therefore the increase of the fluid entropy.

It is seen in Fig. 18 that at $\eta = 1$ the increase of the Hartman number from 20 to 40 results in the augmentation of the entropy generation number N_s from 261.3 to 646.2. This means that by 100% increase of the Hartman number, N_s values increase 147.34%.

The dimensionless entropy generation number profiles for different values of Reynolds number are plotted in Fig. 19. It can be seen that the N_s profiles shift upward (the N_s values increase) with the increase of the Reynolds number. It can be said that by the increase of the Reynolds number, the fluid velocity increases which causes the fluid particles randomness level to increase.

It is seen from Fig. 19 that at $\eta = 1$ the increase of the Reynolds number from 200 to 400 causes the increase of N_s from 214.4 to 261.5, which means an increase of 21.97% in N_s by 100% increase in Re.

The dimensionless entropy generation number logarithmic profiles for various values of Eckert number is plotted in Fig.

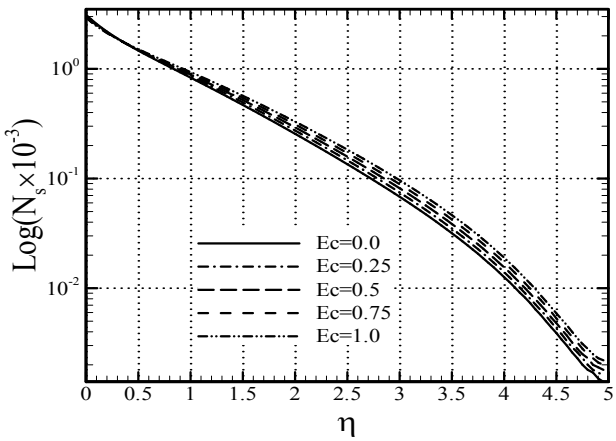

Fig. 20. Dimensionless entropy generation number logarithmic profiles for different values of Eckert number: $Mn = 0.1$, $\varphi = 0.1$, $a_e = 0.5$, $Re = 500$, $\varepsilon = 0.20$, $Ha = 50.0$, $Br\Omega^{-1} = 1.0$, $Pr = 6.2$.

20. It can be seen that for distances closer to the plate surface (η smaller than 0.55) the decrease of Eckert number causes the increase of entropy generation number. When the Eckert number decreases, the difference between plate surface and fluid temperatures boosts. This causes heat transfer enhance ment and therefore increase of fluid particles motion and energy on the plate surface which means the entropy of the fluid passed over the plate has increased. On the other hand, noting Fig. 9 clarifies that the increase of Eckert number causes the increase of temperature in the boundary layer. But according to Fig. 20, this temperature increase, due to increase of Eckert number, shows its influence on a very small distance from plate surface ($\eta \leq 0.55$) when the Eckert number increases from 0.5 to 1.0 directly as the entropy generation increase of the fluid.

It can be seen from Fig. 20 that at $\eta = 0$ when the Eckert number increases from 0.5 to 1.0, the entropy generation number N_s decreases from 3000.1 to 2924.0. This means that when the Eckert number increases 100 % (becomes 2 times larger), then the entropy generation number N_s reduces 2.60%. It can also be seen from Fig. 20 that at $\eta = 1$ when the Eckert number increases from 0.5 to 1.0, then the entropy generation number increases from 885.8 to 934.8, i.e., with the 100% increase of Eckert number the N_s increases 5.53%.

Fig. 21 presents effect of porous medium effective extinction coefficient on dimensionless entropy generation number logarithmic profiles. It can be seen that the entropy generation increases with the increase of effective extinction coefficient a_e. This is due to the fact that when a_e increases, the amount of heat absorption by the fluid in the porous medium increases (see Fig. 10) which strengthens the fluid particle motions in porous medium and therefore the fluid randomness. However it can be said that the effective extinction coefficient does not have considerable effect on the entropy generation number.

It is seen from Fig. 21 that at $\eta = 1$ the increase of the effective extinction coefficient a_e from 1.0 to 2.0 causes the increase of the entropy generation number N_s from 945.9 to

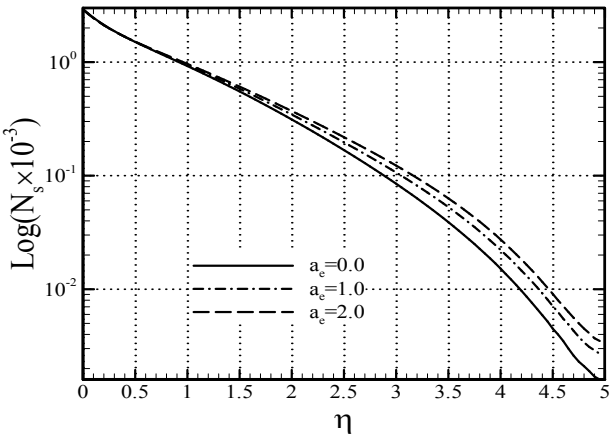

Fig. 21. Dimensionless entropy generation number logarithmic profiles for different values of effective extinction coefficient: Mn = 0.1, φ = 0.1, Re = 500, ε = 0.20, Ha = 50.0, $Br\Omega^{-1}$ = 1.0, Ec = 1.0, Pr = 6.2.

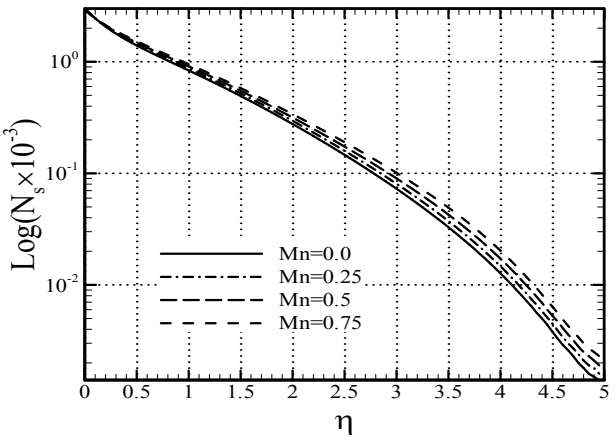

Fig. 22. Dimensionless entropy generation number logarithmic profiles for different values of magnetic parameter: φ = 0.1, a_e = 0.5. Ec = 1.0, Re = 500, ε = 0.20, Ha = 50.0, $Br\Omega^{-1}$ = 1.0, Pr = 6.2.

964.2. This means that 100% increase of a_e causes N_s to increase approximately 1.98%.

Fig. 22 indicates the dimensionless entropy generation number logarithmic profiles for various values of magnetic parameter. It is seen that the magnetic parameter variation cannot considerably affect the N_s profiles such that only a slight upward shifting is observable in N_s profiles with the increase of the magnetic parameter. Therefore, entropy generation number is higher for higher magnetic parameter. The motion of fluid molecules increases in presence of the magnetic force. Therefore the presence of magnetic field in the fluid causes the entropy generation. Moreover, as it can be seen, when the magnetic parameter increases, the effect of this parameter on entropy generation number increase of fluid decreases and becomes almost negligible.

According to Fig. 22, at η = 1 when the magnetic parameter increases from 0.25 to 0.5, then the entropy generation number N_s increases from 872.1 to 910.6 meaning 100% increase in magnetic parameter is equivalent to 4.41% increase in N_s.

6. Conclusions

Entropy generation of magneto hydrodynamic (MHD) mixed convection flow of nanofluid is investigated over a non-linearly stretching inclined transparent plate embedded in a porous medium. The governing equations are transformed into two non-linear coupled ODEs using similarity method. These two equations are then converted into five first order ordinary differential equations. The system of first-order equations are solved by the numerical implicit Keller-Box method. The effects of various parameters such as nanoparticle volume fraction, magnetic parameter, porosity, effective extinction coefficient of porous medium and diameter of porous medium solid particles are studied on the dimensionless velocity, temperature and entropy generation number profiles. The results obtained are as follows:

(1) When the effective extinction coefficient increases, the thermal conditions improve. The presence of nanofluid and also the darkness of solid particles of porous medium in colour can increase the effective absorption coefficient and finally the temperature of thermal boundary layer.

(2) The increase of nanoparticle volume fraction has an enhancement effect on temperature and, in fact, this is the reason for using nanofluids.

(3) Near the plate surface the increase of nanoparticle volume fraction, porosity and porous medium geometric parameter cause the entropy generation number to increase, but far enough from the plate surface the increase of nanoparticle volume fraction, porosity and porous medium geometric parameter cause the reduction of entropy generation number.

(4) The entropy generation number increases with the increase of effective extinction coefficient and magnetic parameter, but it can be said that the variations of effective extinction coefficient and magnetic parameter do not have considerable effect on the entropy generation number.

(5) The variations of Brinkman number and Hartman number show considerable effects on the entropy generation number profiles. The entropy generation number enhances with the increase of Brinkman number and Hartman number, and this increase is more dominant near the plate surface. Therefore low Brinkman and Hartman numbers are more favourable in the MHD flow of nanofluid.

(6) Closer to the plate surface entropy generation number increases with the decrease of Eckert number. However the entropy generation number values increase with the increase of the Reynolds number.

(7) In the case of the velocity profiles, the nanoparticle volume fraction and the Richardson number could be considered as dominant variables since they highly influence the velocity profiles. Nevertheless, in the case of temperature profiles, the effective extinction coefficient and the Richardson number being highly effective on dimensionless temperature variations may be considered the dominant variables. The variations of the Reynolds number, Eckert number, effective extinction coefficient and Magnetic parameter do not considerably affect

the entropy generation number. However, the dimensionless group parameter $Br\Omega^{-1}$, porous medium geometric parameter and the Hartman number may be regarded as the dominant variables for the entropy generation number since their variations could considerably alter the entropy generation numbers.

Acknowledgment

The authors of the paper would like to acknowledge their thanks to Iran Nano-Technology Initiative Council for their financial support. The authors also wish to express their sincerely thanks to the reviewers for their valuable comments and suggestions.

Nomenclature

a : Absorption or extinction coefficient of fluid (m^{-1})
a_e : Effective extinction coefficient of porous media (m^{-1})
b : Stretching rate, positive constant (–)
$B(x)$: Magnetic field (Tesla)
B_0 : Magnetic rate, positive constant (–)
Br : Brinkman number ($=\mu . u_w(x)^2 / \Delta T . k$) (–)
$C(\varepsilon)$: Porous medium inertia coefficient (m^{-1})
C_f : Skin friction coefficient ($=-2f_{\eta\eta}(0)/(\mathrm{Re_x})^{0.5}$) (–)
$(C_p)_f$: Specific heat at constant pressure of the basic fluid ($J\ kg^{-1}\ K^{-1}$)
d_p : Particle diameter (m)
D_p : Geometric parameter of porous medium, positive (–)
Ec : Eckert number ($=u_w(x)^2/C_p(T_w-T_\infty)$) (–)
f : Dimensionless velocity variable ($=\psi(x,y)(\mathrm{Re_x})^{0.5}/u_w(x)$) (–)
g : Gravitational acceleration ($m\ s^{-2}$)
Gr : Grashof number ($=g(T_w-T_\infty)\beta/v^2$) (–)
Ha : Hartman number ($=B_0 x(\sigma/\mu)^{0.5}$) (–)
$K(\varepsilon)$: Porous medium permeability (m^2)
k : Thermal conductivity ($W\ m^{-1}\ K^{-1}$)
m : Index of power law velocity, positive constant (–)
Mn : Magnetic parameter ($=\sigma B_0^2/\rho_\infty b$) (–)
Nu : Nusselt number ($=-(\mathrm{Re_x})^{0.5}\theta_\eta(0)$) (–)
Nu_r : Nusselt number based on radiation heat flux (–)
N_s : Entropy generation number (–)
Pr : Prandtl number ($=\mu C_p/k$) (–)
q_{rad} : Radiation flux distribution ($W\ m^{-2}$)
R : Radiation parameter ($=Nu_r . a_e$) (–)
Re_x : Local Reynolds number ($=\rho . u_w(x)\,x/\mu$) (–)
T : Temperature variable (K)
T_w : Given temperature at the sheet (K)
T_∞ : Temperature of fluid far away from the sheet (K)
ΔT : Sheet temperature (K)
u : Velocity in x-direction ($m\ s^{-1}$)
u_w : Velocity of the sheet ($m\ s^{-1}$)
v : Velocity in y-direction ($m\ s^{-1}$)
X : Horizontal distance (m)
Y : Vertical distance (m)

Greek symbols

ψ : Stream function ($m^2\ s^{-1}$)
η : Similarity variable ($=y(\mathrm{Re_x})^{0.5}/x$) (–)
υ : Kinematic viscosity ($m^2\ s^{-1}$)
β^t : Thermal expansion coefficient (K^{-1})
ε : Porosity of porous medium, positive (–)
μ : Dynamic viscosity ($N\ s\ m^{-2}$)
ρ : Density ($kg\ m^{-3}$)
σ : Electric conductivity ($mho\ s^{-1}$)
θ : Dimensionless temperature variable ($=T-T_\infty/T_w-T_\infty$) (–)
φ : Solid volume fraction, positive (–)
α : Thermal diffusivity ($m^2\ s^{-1}$)
β : Plate inclination angle degrees (–)
ρC_p : Heat capacitance ($J\ m^{-3}\ K^{-1}$)

Subscripts

∞ : Infinity
f : Fluid
nf : Nanofluid
sf : Nanoparticle
w : Plate surface

References

[1] A. Bejan and D. Poulikakos, The non-Darcy regime for vertical boundary layer natural convection in a porous medium, *International Journal of Heat and Mass Transfer*, 27 (5) (1984) 717-722.
[2] J. H. Merkin, Mixed convection boundary layer flow on a vertical surface in a saturated porous medium, *Journal of Engineering Mathematics*, 14 (4) (1980) 301-313.
[3] A. J. Chamkha, Solar radiation assisted natural convection in uniform porous medium supported by a vertical flat plate, *ASME Journal of Heat Transfer*, 119 (1) (1997) 89-96.
[4] H. S. Takhar and O. A. Beg, Effects of transverse magnetic field, Prandtl number and Reynolds number on non-Darcy mixed convective flow of an incompressible viscous fluid past a porous vertical flat plate in a saturated porous medium, *International Journal of Energy Research*, 21 (1) (1997) 87-100.
[5] S. S. Tak, R. Mathur, R. K. Gehlot and A. Khan, MHD free convection-radiation interaction along a vertical surface embedded in Darcian porous medium in presence of Soret and Dufour's effects, *Thermal Science*, 14 (1) (2010) 137-145.
[6] P. Ranganathan and R. Viskanta, Mixed convection boundary layer flow along a vertical surface in a porous medium, *Numerical Heat Transfer*, 7 (3) (1984) 305-317.
[7] P. V. S. N. Murthy, S. K. Mukherjee, D. Srinivasacharya and P. V. S. S. S. R. K. Warangal, Combined radiation and mixed convection from a vertical wall with suction/injection in a non-Darcy porous medium, *Acta Mechanica*, 168 (3) (2004) 145-156.
[8] S. U. S. Choi, Enhancing thermal conductivity of fluids with nanoparticles, *Proc. of ASME International Mechanical En-*

gineering Congress and Exposition, San Francisco, California, USA (1995) 99-105.

[9] S. U. S. Choi, Z. G. Zhang, W. Yu, F. E. Lockwood and E. A. Grulke, Anomalously thermal conductivity enhancement in nanotube suspensions, *Applied Physics Letters*, 79 (14) (2001) 2252-2254.

[10] B. Ghasemi and S. M. Aminossadati, Natural convection heat transfer in an inclined enclosure filled with a water-CuO nanofluid, *Numerical Heat Transfer; Part A: Applications*, 55 (8) (2009) 807-823.

[11] S. E. B. Maiga, S. J. Palm, C. T. Nguyen, G. Roy and N. Galanis, Heat transfer enhancement by using nanofluids in forced convection flow, *International Journal of Heat and Fluid Flow*, 26 (4) (2005) 530-546.

[12] X. Q. Wang and A. S. Mujumdar, A review on nanofluids - Part I: theoretical and numerical investigations, *Brazilian Journal of Chemical Engineering*, 25 (4) (2008) 613-630.

[13] M. Habibi Matin, M. Dehsara and A. Abbassi, Mixed convection MHD flow of nanofluid over a non-linear stretching sheet with effects of viscous dissipation and variable magnetic field, *Mechanika*, 18 (4) (2012) 415-423.

[14] A. Noghrehabadi, M. R. Saffarian, R. Pourrajab and M. Ghalambaz, Entropy analysis for nanofluid flow over a stretching sheet in the presence of heat generation/absorption and partial slip, *Journal of Mechanical Science and Technology*, 27 (3) (2013) 927-937.

[15] S. Ahmad and I. Pop, Mixed convection boundary layer flow from a vertical flat plate embedded in a porous medium filled with nanofluids, *International Communications in Heat and Mass Transfer*, 37 (8) (2010) 987-991.

[16] M. Dehsara, M. Habibi Matin and N. Dalir, Entropy analysis for MHD flow over a non-linear stretching inclined transparent plate embedded in a porous medium due to solar radiation, *Mechanika*, 18 (5) (2012) 524-533.

[17] S. Aboud and S. Saouli, Entropy analysis for viscoelastic magneto-hydrodynamic flow over a stretching surface, *International Journal of Non-Linear Mechanics*, 45 (5) (2010) 482-489.

[18] M. H. Yazdi, S. Abdullah, I. Hashim and K. Sopian, Entropy generation analysis of open parallel microchannels embedded within a permeable continuous moving surface: application to magneto-hydrodynamics (MHD), *Entropy*, 14 (1) (2012) 1-23.

[19] M. Habibi Matin, M. R. H. Nobari and P. Jahangiri, Entropy analysis in mixed convection MHD flow of nanofluid over a non-linear stretching sheet, *Journal of Thermal Science and Technology*, 7 (1) (2012) 104-119.

[20] M. A. A. Hamad, I. Pop and A. I. Md. Ismail, Magnetic field effects on free convection flow of a nanofluid past a vertical semi-infinite flat plate, *Nonlinear Analysis: Real World Applications*, 12 (3) (2011) 1338-1346.

[21] A. J. Chamkha, C. Issa and K. Khanafer, Natural convection from an inclined plate embedded in a variable porosity porous medium due to solar radiation, *International Journal of Thermal Sciences*, 41 (1) (2002) 73-81.

[22] S. M. Aminossadati and B. Ghasemi, Natural convection cooling of a localised heat source at the bottom of a nanofluid-filled enclosure, *European Journal of Mechanics B/Fluids*, 28 (5) (2009) 630-636.

[23] D. Poulikakos and K. Renken, Forced convection in a channel filled with porous medium, including the effects of flow inertia, variable porosity and Brinkman friction, *ASME Journal of Heat Transfer*, 109 (4) (1987) 880-888.

[24] S. P. Anjali Devi and M. Thiyagarajan, Steady non-linear hydromagnetic flow and heat transfer over a stretching surface with variable temperature, *Heat and Mass Transfer*, 42 (8) (2006) 671-677.

[25] T. C. Chiam, Hydromagnetic flow over a surface stretching with a power law velocity, *International Journal of Engineering Science*, 33 (3) (1995) 429-435.

[26] L. C. Woods, *The Thermodynamics of Fluid Systems*, Oxford University Press, Oxford, UK (1975).

[27] M. Z. Salleh, R. Nazar, N. M. Arifin and I. Pop, Numerical solutions of forced convection boundary layer flow on a horizontal circular cylinder with Newtonian heating, *Malaysian Journal of Mathematical Sciences*, 5 (2) (2011) 161-184.

[28] F. S. Ibrahim and M. A. A. Hamad, Group method analysis of mixed convection boundary layer flow of a micropolar fluid near a stagnation point on a horizontal cylinder, *Acta Mechanica*, 181 (1) (2006) 65-81.

Mohammad Dehsara received his B.Sc. in Mechanical Engineering from K.N.T. University of Technology, Iran in 2009. As an outstanding B.Sc. graduate, he exempted from the nationwide M.Sc. entrance exam, also got scholarship from Amirkabir University of Technology (Tehran Polytechnic) to pursue his M.Sc. in Mechanical Engineering. In 2012, he graduated from Amirkabir University of Technology in Energy Conversion field. Currently, he is a Ph.D. candidate in the School of Mechanical and Materials Engineering at the Washington State University.

Nemat Dalir received his B.Sc. and M.Sc. degrees in Mechanical Engineering from Tabriz University, Tabriz, in Iran, and Iran University of Science and Technology (IUST), Tehran, in Iran, in 2008 and 2010, respectively. He is currently at the edge of receiving his Ph.D. in Mechanical Engineering from Department of Mechanical Engineering at Amirkabir University of Technology (Tehran Polytechnic), Tehran, in Iran. His research program is in the field of hydrodynamic instability. He also teaches part-time at Salmas Branch of Islamic Azad University, Salmas, in Iran.